RE-VISITING YOLLA – NEW INSIGHTS ON SPUDCAN PENETRATION

Erbrich C.T.*, Amodio A, Krisdani H., Lam S.Y. and Xu X.
Fugro AG Pty Ltd

Tho. KK.
Fugro Singapore Pte Ltd

* *corresponding author:c.erbrich@fugro.com*

1 ABSTRACT

In 2004 the Ensco 102 was spudded alongside the Yolla A platform in the Bass Strait, Australia. The uncemented silty carbonate soils at this site resulted in several surprises and insights which were documented and discussed in Ref [1], including deeper than expected penetration and unexpected punch-through events which were both driven by the very high sensitivity of the soil and the transitional drainage conditions. In early 2015 the Seadrill West Telesto was brought alongside the Yolla A platform with its spudcans re-penetrated through the existing craters. An extensive engineering exercise was commissioned to minimise the risk of any 'surprises' this time. This included extensive site investigations of the crater in-fill material, including CPT, ball penetrometer and laboratory testing. Detailed re-analysis of the original penetration and of the planned re-penetration process was also undertaken using new analytical tools and through large deformation finite element analysis. This paper presents these assessments in detail and compares the predictions made with the penetration measured in the field.

KEY WORDS: Yolla, Carbonate, Punch-through, Storm Stability, LDFE, ABAQUS CEL

2 INTRODUCTION

The Yolla field is located in the Bass Strait, offshore Australia, due east of King Island and due North of Burnie, Tasmania. The field was first developed in 2004 with an unmanned platform (Yolla A), founded on a large skirted raft in order to produce gas for export by pipeline to Kilcunda in Victoria. The production wells for this platform were spudded in mid 2004 using the Ensco 102 (E102) jack-up rig, which was brought alongside Yolla A shortly after the platform installation. The three spudcans penetrated to between about 23 m and 24 m below mudline under the maximum applied preload, which was significantly deeper than expected and, in addition, unexpected punch-throughs with long leg-runs were experienced leading to rig tilts and near collisions with the Yolla A platform. Following completion of drilling, the E102 jack-up rig was demobilised, resulting in the formation of large seabed craters (typically around 38 m diameter at original mudline x 6 m deep and each with an excavated volume of around 3,300 m^3).

Recently, Origin Energy Resources Limited (Origin) has undertaken the Mid-life Enhancement (MLE) Project, which included an upgrade of the facilities onboard the Yolla A Platform and the drilling of additional wells. For the drilling operation, a Friede and Goldman JU 2000E class rig (Seadrill West Telesto) has been used for a new work-over operation in the existing craters. The West Telesto has a very similar spudcan layout and geometry as the E102 and was selected to minimise crater interaction issues. Importantly, the additional Yolla A facilities have extended the deck footprint towards the jack-up location, which imposes additional restrictions on permissible rig displacements during any punch-through, in order to avoid collisions.

The original Yolla operations were described in Ref [1], including an explanation for the unexpected penetration behaviour. In the current paper, the studies performed to plan for the recent re-penetration operation are presented. Extensive site investigation activities were conducted to determine the properties of the crater in-fill material. This was followed

by spudcan penetration analyses which were conducted using analytical tools and large deformation finite element (LDFE) analysis. The original Ensco 102 results were also revisited in order to calibrate the models. The results of all these investigations are presented in this paper.

3 SITE INVESTIGATION AND TESTING PROGRAMMES

Both the in situ and crater infill material have been extensively investigated during multiple site investigations conducted by Thales, Fugro and Benthic Geotech. Field testing has comprised CPT, T-bar and ball penetrometer tests, with the latter two comprising both static and cyclic tests. Extensive laboratory testing has also been performed on recovered samples which has included assessments of monotonic strengths (intact and remoulded), cyclic strengths and consolidation properties as well as standard classification testing.

4 SOIL CONDITIONS – IN SITU CONDITIONS

The in situ material is laterally homogeneous but exhibits significant variability with depth. The site generally comprises a variety of interbedded layers of uncemented carbonate sand/ silty sand/ sandy silt but also includes a number of calcareous clay layers. A typical in situ CPT profile, annotated with the stratigraphy, is shown on Figure 1. The penetrometer results in the carbonate silty sand/ sandy silt layers exhibit varying degrees of partial drainage which complicates interpretation of the strength. These materials are also highly sensitive, with measured sensitivity (S_t) around 10 to 20. In contrast, S_t of the calcareous clay layers is only around 4. Further details are presented in Ref [1].

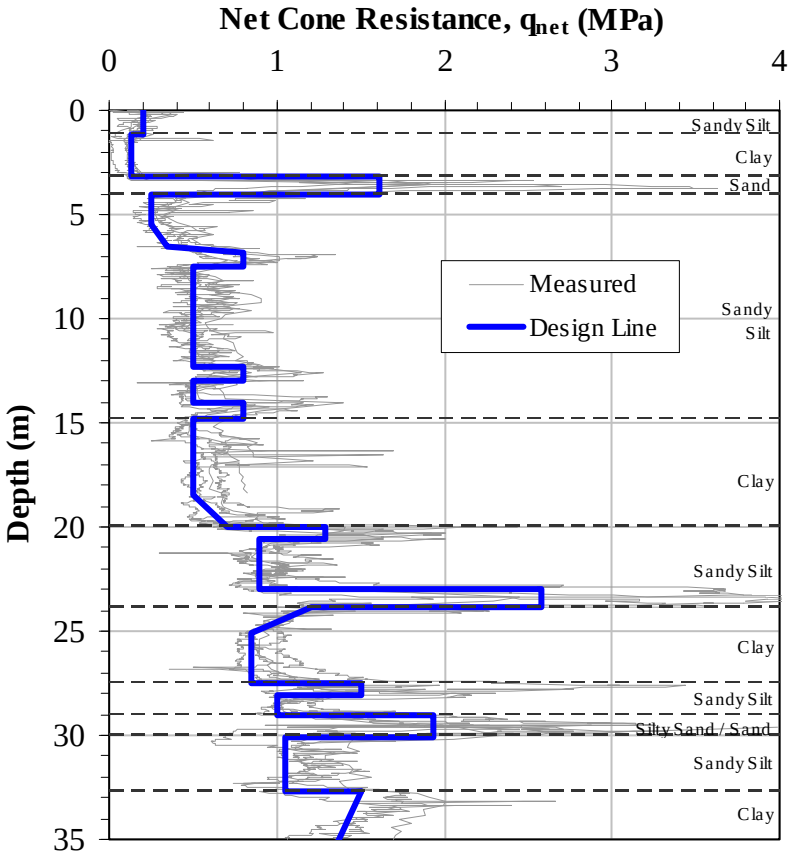

Figure 1: A Typical In-situ CPT Profile

5 SOIL CONDITIONS – CRATER INFILL MATERIAL

The first investigation of the crater infill material comprised a single CPT probe through the centre of each crater, along with static and cyclic ball penetrometer tests in the port and bow craters. The CPT response obtained in each of these craters is presented on Figure 2. It can be observed that there is significant variability between the three craters, with the starboard crater exhibiting a typically sandier response than the other two craters. The greater presence of sand in this crater was thought to be due to the more extensive use of jetting during extraction of the E102 spudcan compared to the other craters. Initial analyses indicated a punch-through risk at this crater during re-penetration and hence it was decided to collect additional data from this location, which comprised a series of CPT's scattered across the crater. Figure 3 illustrates the results from these additional investigations. It can be seen that while the original centre CPT exhibits the greatest prevalence of sand, significant zones of potentially interconnected sand exist across this crater.

An interesting finding from the laboratory test programme is that the sensitivity of the remoulded/ reconsolidated crater infill material was generally much lower than the original in situ material; typically S_t was measured as around 4.

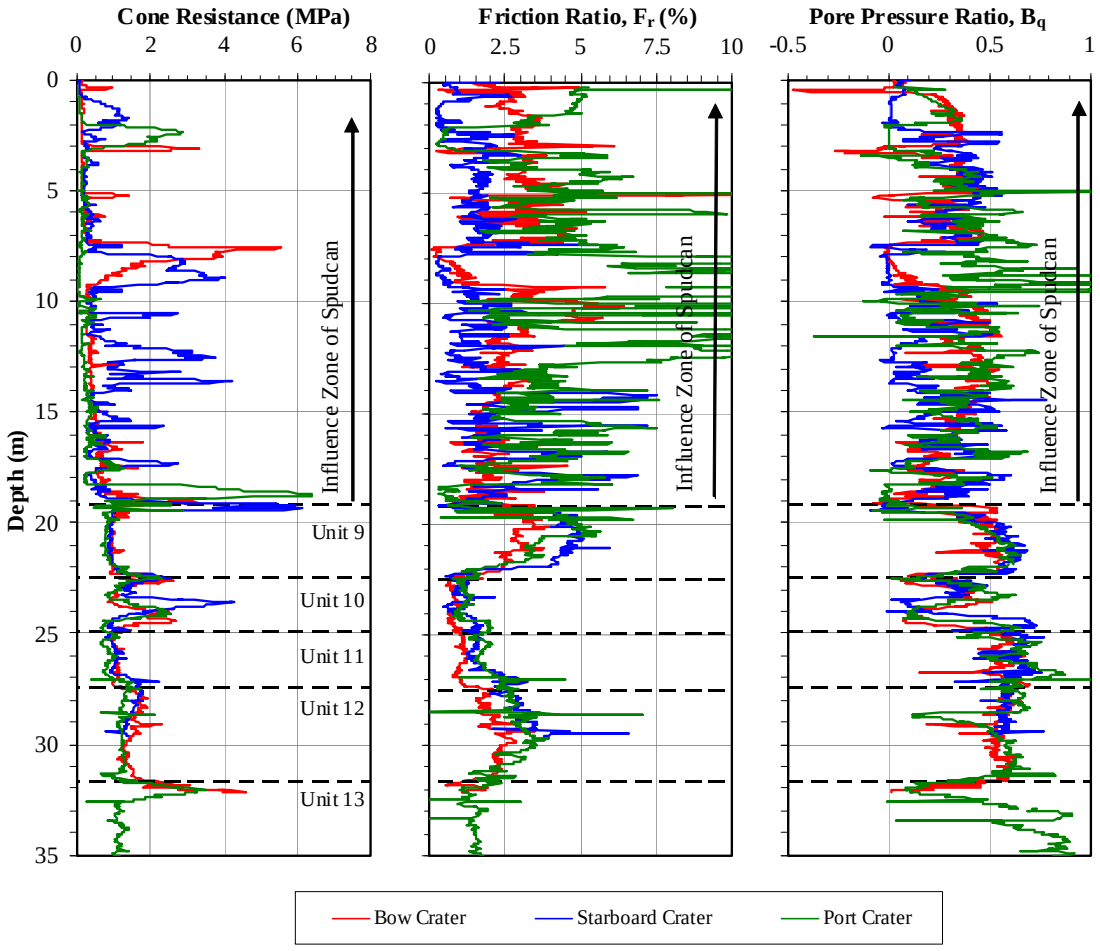

Figure 2: CPT response obtained in Bow, Starboard & Port Crater

6 SHEAR STRENGTH - IN SITU SOIL

One of the major challenges for the re-penetration assessment was the assignment of appropriate soil strengths. As noted above, the penetrometer results exhibit varying drainage conditions. In addition, as discussed in Ref [1], during spudcan penetration the

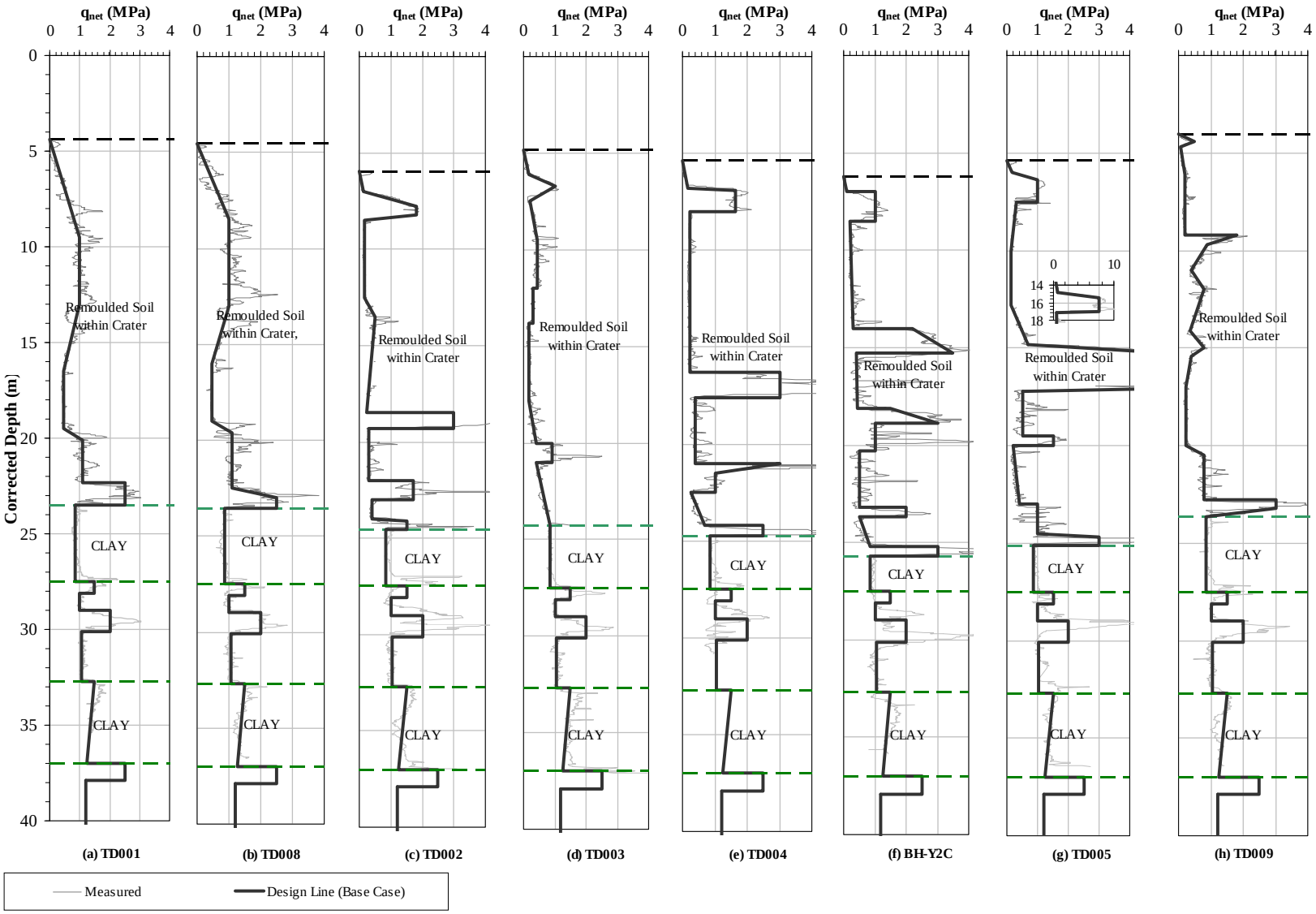

Figure 3: Additional PCPT Data Obtained Within Starboard Crater (refer to Figure 14 for CPT locations)

degree of drainage is generally expected to be lower (i.e. closer to fully undrained) than during a penetrometer test. The reference strength to be used in these assessments is therefore the fully undrained strength, subject to certain modifications for partial drainage where appropriate, as discussed later.

The undrained strength (s_u) can be defined from the CPT resistance as $s_u = q_{net}/ N_k$ where q_{net} is the net cone resistance and N_k is the cone factor. For the in situ carbonate soil, various methods were considered for defining N_k, to account for the effects of partial drainage, but in this paper we will only present the final preferred model, termed the "Variable N_k model Mk-II". In this model N_k is defined as:

$$N_k = A + B\frac{q_{net(CPT)}}{\sigma'_{vo}} \quad \text{with } C \le N_k \le D \tag{1}$$

where C = 15 and D = 40 represent the assigned limits of N_k that apply for fully undrained and fully drained CPT conditions respectively. The parameters A and B are calculated as variable functions of depth as shown on Figure 4. The selected form of these relationships is based on the general observed response in typical carbonate soils and to give the best calibration to the available strength data. For the calcareous clay layers a constant N_k of 15 was adopted throughout, reflecting the inherently undrained nature of CPT penetration through such soils. The resulting undrained strength profile derived for the in situ soil is presented on Figure 5, based on the design q_{net} profile presented on Figure 1.

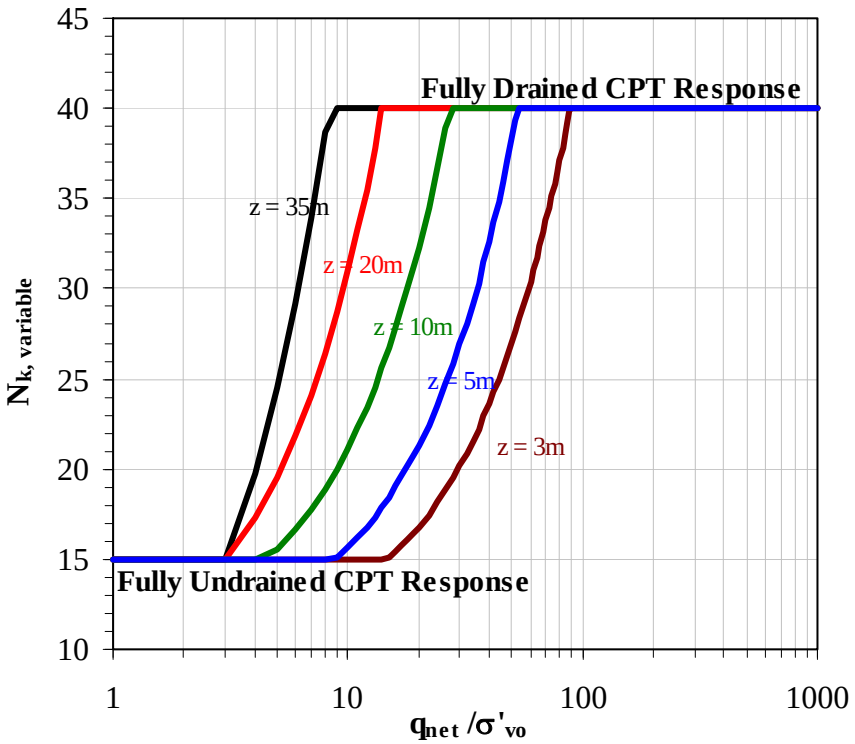

Figure 4: Variation of Parameter A and B as a Function with Depth (Variable N_k Model Mk-II)

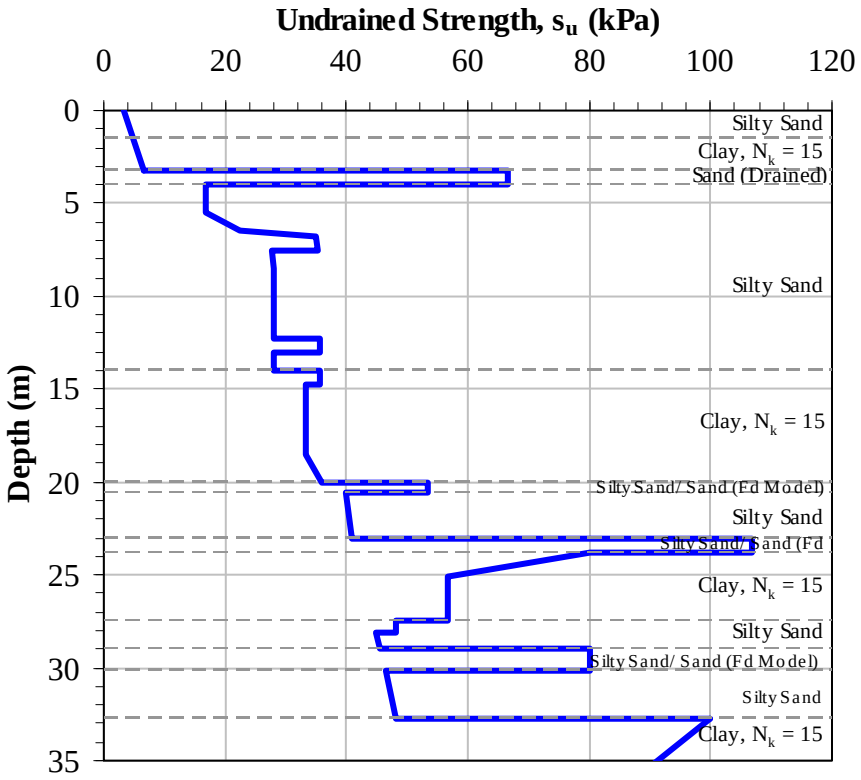

Figure 5: Insitu Undrained Peak Strength Profile

Equation 1 defines the pure undrained shear strength of the soil profile. However, a few of the layers in the virgin soil profile (i.e. at around 3.5 m, 20 m, 24 m and 30 m), exhibit a relatively high coefficient of consolidation, c_v. In these layers, the assumption of fully undrained behaviour during spudcan penetration will result in an excessively low penetration resistance. For the upper layer at around 3.5 m, the c_v is sufficiently high that it is expected to respond in a close to fully drained manner during spudcan penetration and hence a purely frictional model is more appropriate.

For the other three deeper sandier layers, partially drained conditions are expected during spudcan penetration. For these three layers we have retained the cohesive strength model but have defined the "strength" using an N_k of 15/0.62 = 24.2, where 15 is the selected N_k for fully undrained CPT conditions (see Figure 4) and 0.62 represents a drainage correction factor as defined in Ref [1]. The "shear strength" resulting from this model is somewhat higher than the pure undrained strength derived with the variable N_k model Mk-II, but is less than implied using a fully drained frictional model.

7 SHEAR STRENGTH – REMOULDED CRATER INFILL MATERIAL

Consolidation testing of the crater infill material revealed that for the majority, the value of c_v had reduced from typically 7,000 m^2/yr for the in situ state to around 100 m^2/yr after remoulding and reconsolidation. In this material, fully undrained conditions therefore apply for both CPT and spudcan penetration and hence an N_k of 15 was found applicable to assess the undrained strength. At a number of places, particularly in the starboard crater, much more sandy material is apparent (i.e. where q_{net} exceeds about 1 MPa). In such materials the CPT appears to have responded in a fully drained manner and hence the much larger spudcan might respond in a similarly drained way or may exhibit partially drained to undrained behaviour, depending on the exact consolidation properties that apply to these layers. Unfortunately we did not have sufficient information to accurately evaluate this and hence since our principal concerns were associated with punch-through or premature refusal, it was more conservative to assume that these layers would respond in a fully drained manner during spudcan penetration.

8 JACK-UP DETAILS

The Ensco 102 is a Keppel FELS Mod V "A" class jack-up rig while the West Telesto is a Friede and Goldman JU2000 E class jack-up. The widest diameter (D) of the Ensco 102 spudcans is 18.2 m and the total base area of each spudcan is 259.8 m^2. During the 2004 operations at Yolla a maximum static preload of 97.8 MN was applied. The West Telesto spudcans are virtually identical, with a widest D of 18 m and a base area of 253.9 m^2. Although a preload up to 112 MN can be applied, it was decided that in most scenarios the maximum static preload would be limited to 90 MN for the planned operations at Yolla.

9 ANALYTICAL PENETRATION MODEL – DESCRIPTION

In reviewing the unexpected penetrations at Yolla during the 2004 operations, Ref [1] presented a procedure for assessing the spudcan resistance directly from penetrometer results, specifically in that case, T-bar results. However, the CPT is the most commonly performed penetrometer test since it can be conducted in the widest variety of soil types. While T-bar and ball penetrometer tests have been conducted within the in situ and crater infill materials at Yolla, the majority of the available field tests are CPT. To assess the spudcan penetration resistance at Yolla we therefore used the CPT resistance (q_{net}) as the reference. The spudcan penetration resistance ($Q_{spudcan}$) is then calculated as:

$$Q_{spudcan} = \left(\frac{q_{net}}{N_k} \right)_{ave} \cdot N_c \cdot A_{spudcan} \tag{2}$$

where N_k are the cone factors derived as discussed in Section 6 and 7, A is the spudcan base area and N_c is a bearing capacity factor defined as:

$$N_c = \min\left(N_{c-\min} + \frac{N_{c-\lim} - N_{c-\min}}{S_t} \cdot \frac{z/D}{(z/D)_{\max}}, N_{c-\lim} \right) \tag{3}$$

where $N_{c\text{-}min}$ and $N_{c\text{-}lim}$ are lower and upper limits on bearing capacity factor respectively (equal to 6.05 and 11.00), $(z/D)_{max}$ is the depth to diameter ratio at which $N_{c\text{-}lim}$ is reached (assumed to be 2.5), sensitivity S_t is assigned values of 10 for in situ soil and 4 for remoulded crater material) and z is the penetration depth. In Equation 2, $(q_{net}/N_k)_{ave}$ denotes that the average value over the depth of the failure zone is used to assess the penetration resistance.

Punch-through checks were also performed using the 1:3 load spread method in accordance with the procedure presented in Ref [2], and squeezing checks were also conducted for weak layers underlain by stronger material using a squeezing factor derived from Ref [3] for homogeneous soils, which is very similar to the squeezing factor proposed in Ref [2].

10 ANALYTICAL PENETRATION MODEL – RESULTS

Using the aforementioned analytical model, spudcan penetration resistance vs. depth profiles have been developed for the original intact soil (E102) and for the CPT's through the centre of each crater (West Telesto). The design q_{net} profiles used in each case are included on Figures 1 and 2 while the predicted spudcan penetration resistance results are presented on Figures 6 and 7, respectively. The measured 2004 penetration results for the E102 are also shown on Figure 6, along with a more complete set of "inferred penetration results", as derived by Rupert Hunt (retained by Origin to provide specialist support), after some additional post-processing of the original installation records. The latter revealed a previously unreported essentially simultaneous leg run on all legs between 7 m and 16 m penetration under an applied pre-load of 55 MN. It is unclear why this did not cause any alarm in 2004, but most likely this is because it was a single event which was over very quickly, resulted in no tilt of the rig and also occurred well above the final penetration

depth. This contrasts with the later leg runs that occurred during leg-by-leg preloading with the hull in the water when the preload was about 85 MN, leading to runs between 2.5 m and 5 m at the different legs, in turn inducing tilts up to 4 degrees and leading to the rig coming within 3 m of contacting the Yolla A platform (Ref [1]).

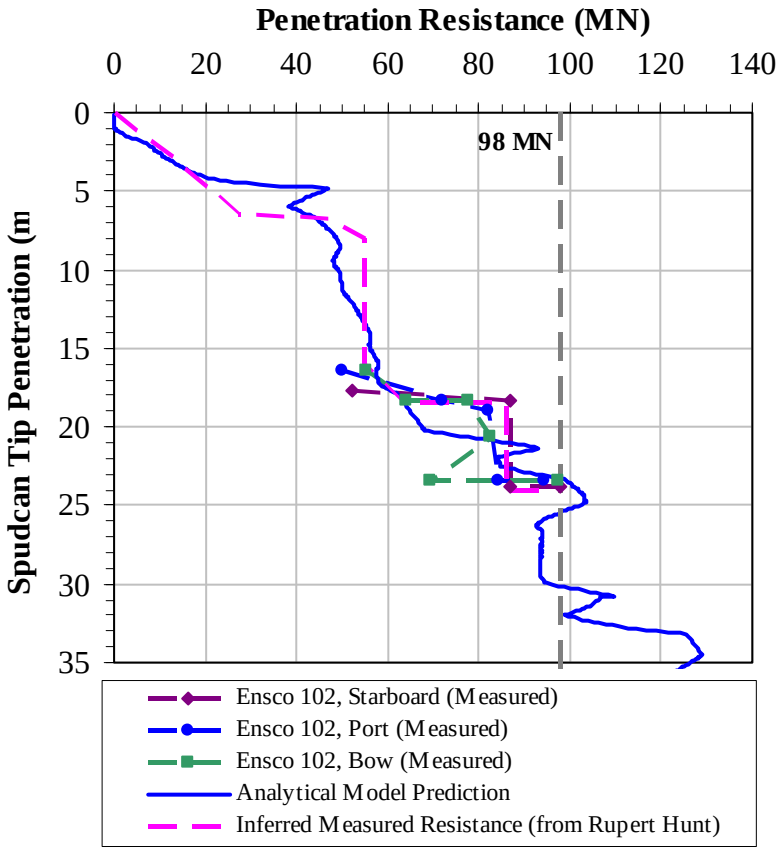

Figure 6: Spudcan Penetration Resistance for E102 Virgin Penetration

It can be seen that the analytical model represents a fair but not perfect match to the measured data for the E102. In particular the upper leg run is predicted to commence at a shallower depth and is shorter than apparently observed, while the prediction for the later leg run reasonably matches the least onerous measured case (bow leg) but underestimates the longer leg runs at the other two legs.

Within the craters (Figure 7) it can be seen that a wide range of response is predicted for the West Telesto, but a common feature is that the final penetration depth is around 23 m in all cases. A number of potential leg runs can also be observed, but provided these were to occur at leg loads below the self weight of the jack-up then the rig remains floating which prevents a true punch-through; instead the legs are simply jacked down against a reducing resistance which slightly changes the hull draft in the water. Given the general risk of leg runs, the project elected to adopt an unusual but effective procedure, whereby before the rig was soft-pinned it would be ballasted to the maximum permissible level which still allowed simultaneous leg jacking with the hull in the water. For the West Telesto this was determined to be 70 MN per leg, which is only 20 MN short of the target final preload of 90 MN; this essentially mitigated most punch-through risks, except at the starboard crater.

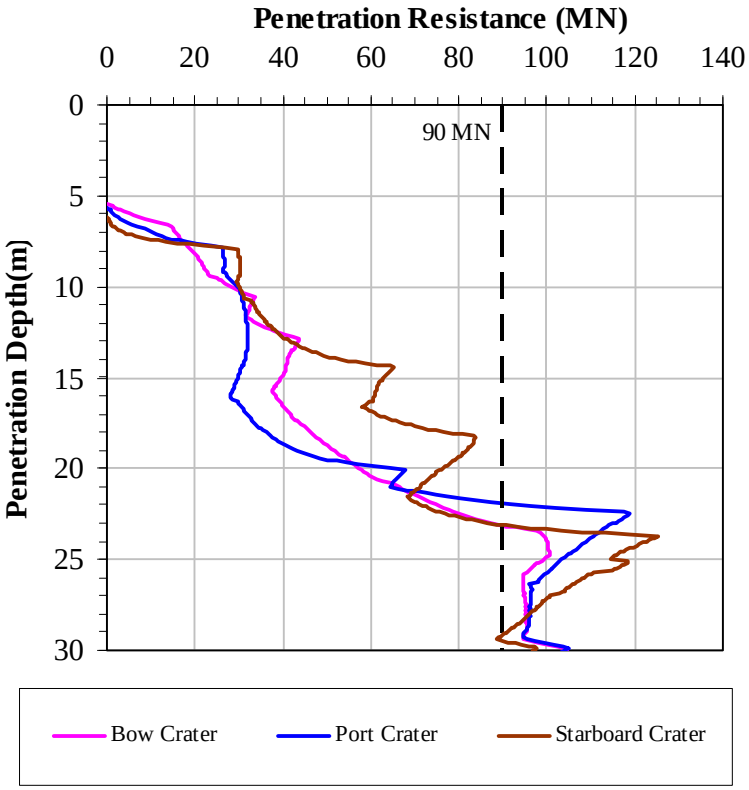

Figure 7: Spudcan Penetration Resistance for Bow, Port and Starboard Crater

As noted earlier, the maximum preload of 90 MN was limited to well below the maximum permissible value of 112 MN; the reason for this is apparent from the results presented on Figure 7; a high punch-through risk with long leg drops is evident under such high preloads and this could not be safely managed. In this regard it is interesting to note that the predicted margin against a further punch-through of the E102 under the maximum applied 98 MN applied is uncomfortably small and would have been cause for concern if known at the time. Fortunately, no such event occurred, and hence this provided significant reassurance that such an event would not occur with the West Telesto at a similar predicted margin. However, there remained some uncertainty as to exactly what influence the E102 spudcan extraction operation may have had on the properties of the underlying soil and hence the increased margin implied with the selected 90 MN maximum preload was deemed a pragmatic risk reduction measure.

The results presented above for the starboard crater only considered the central CPT but show a very ugly looking punch-through risk at around 80 MN preload, amongst others. In addition, it was considered that the significant number of apparent thin sand "layers" could give rise to a potential for "clumping" together into a larger conglomeration, by squeezing out of the intervening weak layers. While this might reduce the punch-through risk it could also lead to a shallower penetration at which it may have been difficult to prove an acceptable capacity under the design 50 year storm load (Ref [4]). Despite these concerning observations, it was thought highly unlikely that the central CPT would be a representative average of the entire infill material at this crater and on this basis it was decided to further investigate the material in this crater.

As noted earlier, the results of the additional CPT probing in the starboard crater are presented on Figure 3; a design profile used in the subsequent penetration resistance assessments performed is also shown on each. The key question is how to combine the results from these individual probes into an "average" response applicable to the West Telesto spudcans. To this end we considered two alternative weighting procedures for combining results:

Method 1 - spudcan penetration resistance estimated from the weighted average of the resistance calculated for each individual CPT profile, i.e.:

$$Q_{spudcan(Average)} = \frac{\sum\left(w_i \cdot Q_{spudcan-i}\right)}{\sum w_i} \tag{4}$$

where $Q_{spudcan\text{-}i}$ = penetration resistance calculated from individual CPT's using the full spudcan D.

Method 2 - spudcan penetration resistance estimated from sum of resistance calculated based on an appropriate weighted area for each individual CPT profile, i.e.:

$$Q_{spudcan(Average)} = \sum Q_{spudcan-i} \tag{5}$$

where $Q_{spudcan\text{-}i}$ = penetration resistance calculated from individual CPTs using a weighted spudcan diameter $D_i = w_i^{0.5} \cdot D$; in essence a number of 'mini-spudcans' are assumed in the calculations. In both methods w_i = weighting factor for individual CPT's based on their tributary area and D is the spudcan diameter.

The selection of values for w_i is somewhat controversial. For this exercise we simply assigned a "zone of influence" around the centre of each measured CPT (as shown by the colour shading on Figure 14); in essence we assumed that these are random results with no underlying order. It has been suggested that this assumption is too crude and there should be a detectable and systematic order to the measured CPT results, given the axi-symmetric nature of spudcan penetration within the original in situ soil. While we have some sympathy with this reasoning, we believe that even with the amount of data collected in this case, the state of knowledge remains insufficient to be confident that the required order can be imposed accurately but also sufficiently conservatively for this critical design scenario. As noted earlier, the strong sand "layers" detected in the CPT are principally believed to be due to water jetting during extraction of the E102, and hence are likely concentrated within the cylinder of soil defined by and centred on the spudcan diameter. The key concerns for this project were punch-through and premature refusal, and hence it is reasonable to assume that the "zone of influences" we have assigned would lead to conservative predictions for both these issues, since the modelled strong "sand layers" extend well beyond the cylinder of soil defined by the spudcan diameter, and hence this conservatively reinforces the penetration resistance.

The final result obtained, in terms of the weighted average penetration resistance versus depth proved to be very similar with the two methods, and hence hereon we only present the results obtained with Method 1. The penetration vs. resistance curves for each individual CPT profile as well as the weighted average are presented on Figure 8. It can be seen that while various potential leg runs are identified amongst the various individual results, the weighted average shows a much more benign resistance profile, with no significant leg runs predicted for preloads exceeding the 70 MN hull-in-water simultaneous leg jacking limit.

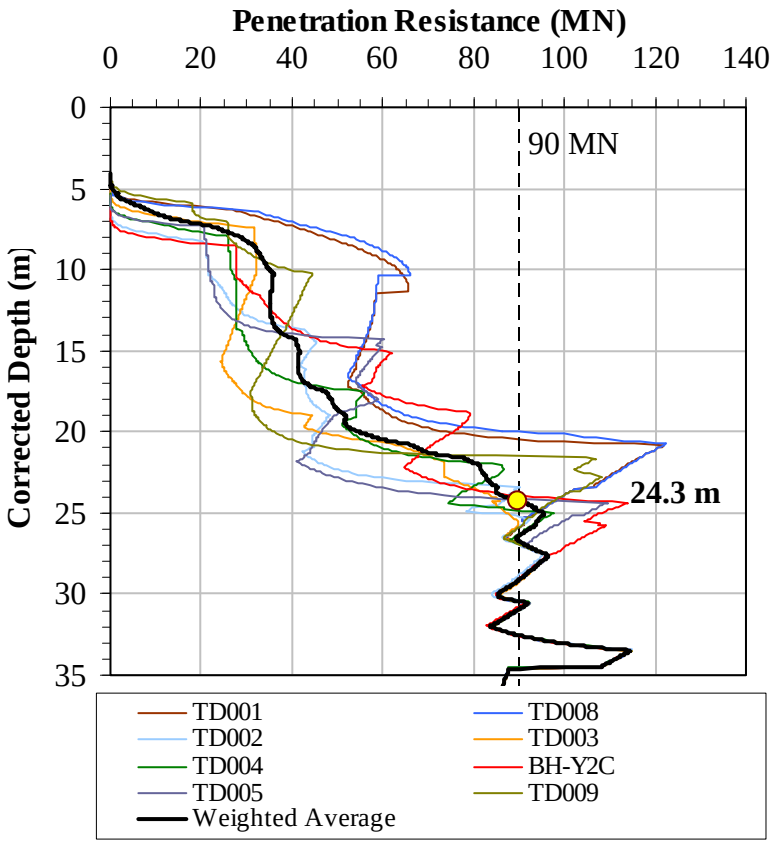

Figure 8: Penetration Resistance Curves for Each Individual CPT Profile (Method 1)

Despite these more optimistic results in terms of leg runs, some concerns were still raised as to whether the adopted averaging procedures could be wholly relied upon. In addition, the analytical solution does not address the risk of "clumping sand" potentially leading to premature refusal. To provide further reassurance on these critical matters the project therefore elected to undertake large deformation finite element analyses using the ABAQUS Coupled Eularian-Lagrangian (CEL) capability (Ref [5]).

11 LDFE MODEL – INTRODUCTION

The ABAQUS CEL capability is principally an Eulerian analysis, which means that the spatial position of the nodes is fixed and the finite element mesh undergoes zero distortion during the analysis. Instead, materials are allowed to move (flow) from one element to another element during the analysis. Owing to the large deformations inherent to deep spudcan penetration problems, the Eulerian approach is an attractive solution strategy since the problems associated with severe mesh distortion in the case of a standard Lagrangian analysis are completely mitigated. The "Coupled Lagrangian" in the method descriptor refers to the ability of an Eularian mesh (the soil) to interact with a separate Lagrangian body (the spudcan in this case).

Reasonable experience has been obtained to date using the CEL method with conventional clays and sands (e.g. Ref [6]); however, to our knowledge this has not previously been applied to such complex stratigraphy and with such highly sensitive soils as encountered at Yolla. Hence before embarking on this exercise it was considered essential to provide some validation of the model performance. To this end we have first analysed the original E102 penetration in virgin soil before addressing the response in the starboard crater.

12 LDFE MODEL – DESCRIPTION & RESULTS; ENSCO 102

The mesh used for the E102 LDFE analysis is presented on Figure 9. A rectilinear mesh comprising cubical 8-noded brick elements (0.4 m dimension) was used throughout the soil zone where spudcan penetration was expected to cause plastic soil flow, but grading to larger elements further away. The top of the mesh was defined at 3 m above mudline (i.e. 3 m of void elements were included to capture soil heave), while the mesh base was defined at 33.6 m below mudline. The element size was selected based on the mesh convergence studies presented in Ref [6] which found that elements with dimensions not exceeding 0.25 m x 0.25 m x 0.25 m were required in the general vicinity of the spudcan in order to model the response of a 12 m diameter spudcan accurately. The element size used for Yolla is a simple pro-rata scaling of this result.

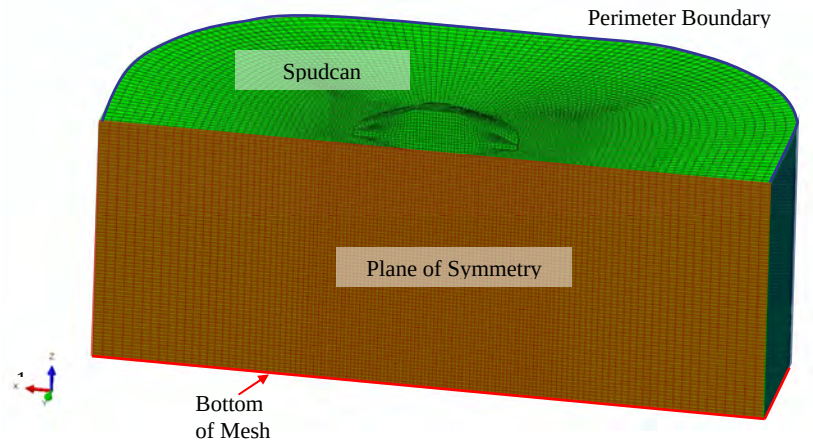

Figure 9: Mesh for E102 LDFE Analysis

The strain softening associated with the large degree of remoulding expected in this case was a critical modelling detail. The approach presented in Ref [7] has been adopted in this case where the following approximate analytical expression is used to evaluate the operative strength as a function of plastic strain:

$$\frac{s_u}{s_{uo}} = \delta_{rem} + \left(1 - \delta_{rem}\right) \cdot e^{-3\gamma_p / \xi_{95}} \qquad (6)$$

where:
- ξ_{95} = $2\xi_p N_{95}$
- s_u = Operative undrained strength
- s_{u0} = Peak strength
- γ_p = Plastic shear strain
- ξ_{95} = Cumulative plastic shear strain required to cause 95% reduction of shear strength (from peak to remoulded)
- ξ_p = Theoretical average shear strain per passage of the penetrometer (typically equal to about 4)
- N_{95} = Number of cycles required to cause 95% reduction of shear strength (from peak to remoulded)

As indicated in Ref [1], typical N_{95} and S_t for Yolla intact sandy silt/ silty sand were 2 and 15 respectively, whereas for clay layers N_{95} and S_t were both assessed to equal 4 from the available T-bar results. The parameter ξ_p is a function of the surface roughness (α) of the T-bar ranging from 3.27 to 4.42 for an α ranging from 1 to 0, respectively; a typical value of ~4 was adopted for the current study. Hence ξ_{95} is calculated to be about 16 and 32 for sandy silt and clay, respectively.

Localization into thin shear bands can develop during a strain softening event, but in a finite element analysis, the minimum thickness of shear band that can develop is controlled by the element thickness. In this case, 0.4 m thick elements were adopted, while it could reasonably be expected that a real shear band could be in the order of 10 times thinner. This can be dealt with by factoring the value of ξ_{95} by the ratio of the element size to the shear band thickness (i.e. in the order of 10 in this case). However, if diffuse shear failure develops in the presence of strain softening (which is often expected in axisymmetric problems, such as circular spudcan penetration) then no scaling of ξ_{95} is required. A series of trial analyses revealed the potential for both diffuse plastic shear and localisation into shear bands, with the latter prominent during punch-through events. The only way to rigorously resolve this conflict would be to use an element size consistent with the shear band width. However, since this is in the order of 10 times smaller than the element size used in the current mesh this is not a feasible proposition with current computer hardware.

A compromise position was therefore required and for the E102 back analysis we finally adopted ξ_{95} as 8 and 15 for the sandy silt and clay respectively. These are approximately half the measured values and hence this represents a "balanced" approach, which allows for some influence of shear band formation, but the rate of strain softening in a shear band will be underestimated.

As indicated earlier, for the upper "sand" layer at around 3.5 m, a drained frictional response was considered appropriate and hence friction and dilation angles of 35° and 5° respectively were assigned to this layer. All other layers were modelled using a Tresca cohesive model, using the peak strength profile presented on Figure 5 and the strain-softening model described above.

The spudcan was modelled as a rigid solid part instead of using deformable brick elements which would have been computationally more time consuming. Spudcan penetration was conducted at a constant velocity, with the spudcan initially positioned at the mudline and progressively pushed downward. While the explicit time integration model represents an inherently dynamic solution, the selected penetration velocity was chosen such that any true dynamic effects would be minimal.

Figure 10 presents static images of the distribution of intact undrained strength at various stages during penetration of the E102 spudcans. Figure 11 presents similar results for the operative strength (i.e. accounting for remoulding).

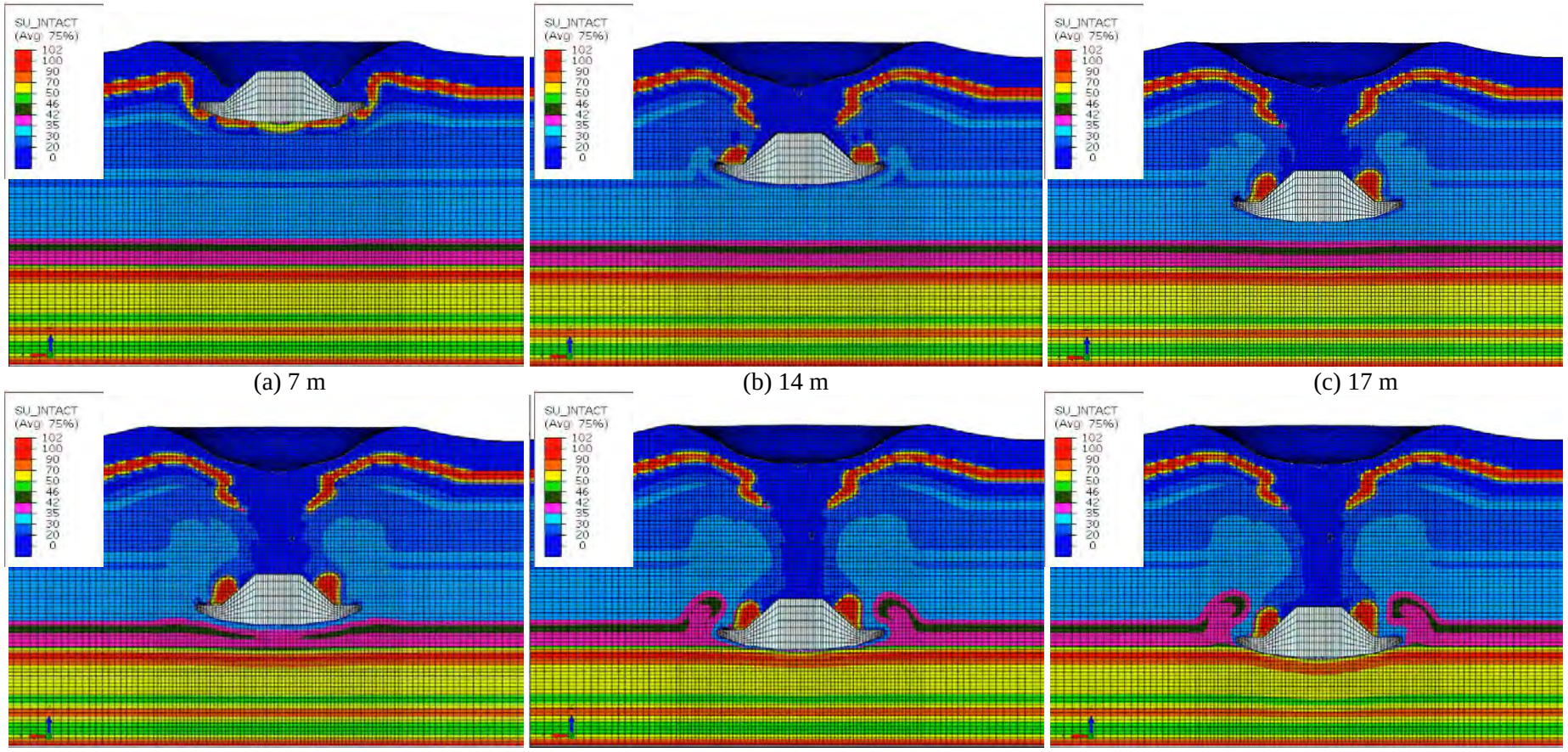

(a) 7 m (b) 14 m (c) 17 m

(d) 20 m (e) 23 m (f) 25 m

Figure 10: Contours of the intact undrained strength on central vertical plane for E102 model

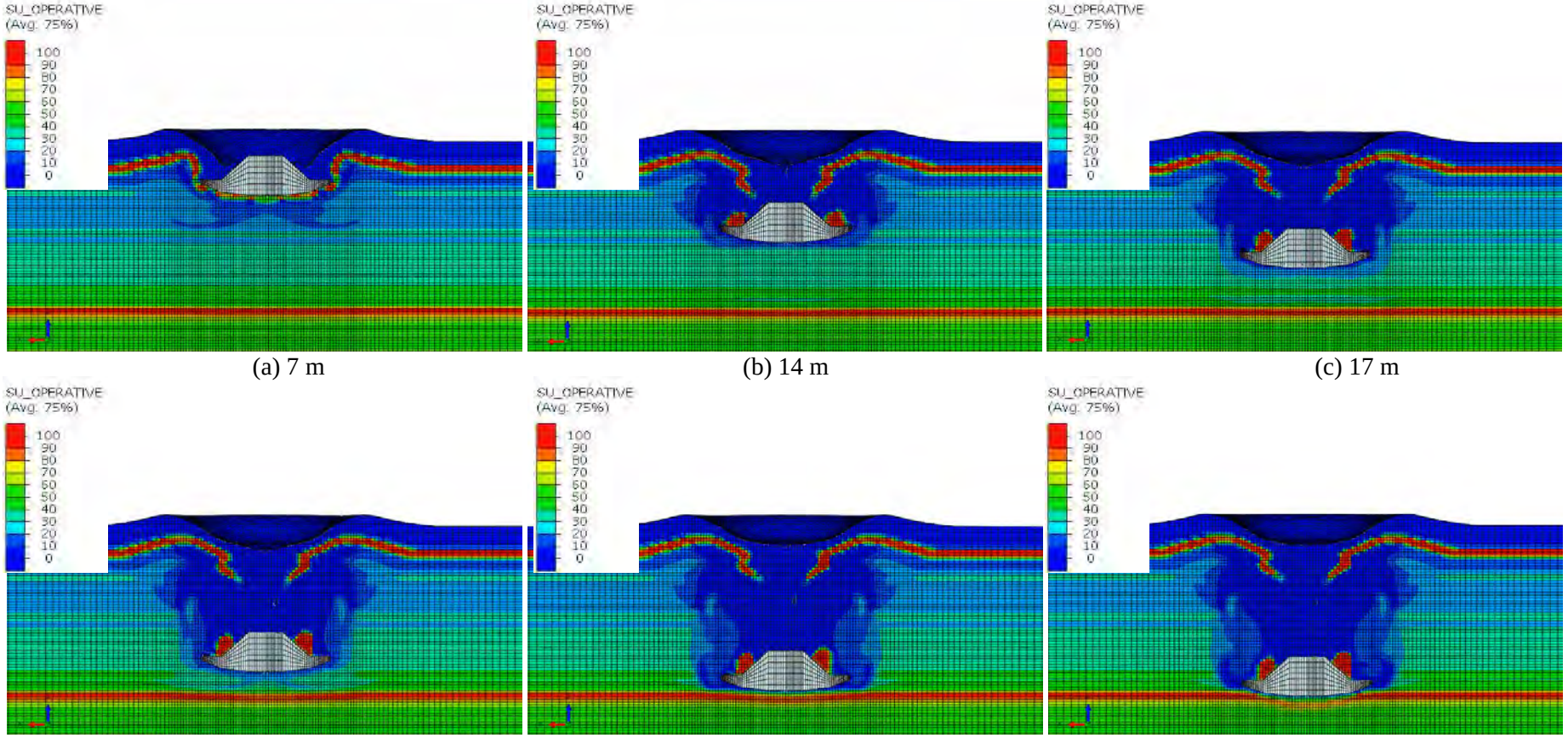

(a) 7 m (b) 14 m (c) 17 m

(d) 20 m (e) 23 m (f) 25 m

Figure 11: Contours of the operative undrained strength on central vertical plane for E102 model

Considering the intact strength, the disorder in the contours around the spudcan is entirely due to material migration and the consequent averaging of multi-material strengths when more than one material type is present within any element. It should be noted that while the upper sand layer has been modelled with frictional material properties, for visualisation purposes it has been assigned a nominal undrained strength of >100 kPa (i.e. higher than all the other layers). This is done only so that movement of the sandy layer can be visually traced and this strength is not used in the analysis itself. Figure 12 presents the accumulated plastic strain contours at the same depths. It can be observed that most of the soil directly above the spudcan has been strained to in excess of 1000% strain (i.e. PEEQVAG = 10), which corresponds to >95% degradation to the fully remoulded strength in the sandy silt and about 85% degradation to the fully remoulded strength in the clay. It can also be seen that the diameter of the significantly disturbed zone extends to between 2.7 times the spudcan diameter near the surface, reducing to about 1.5 times the spudcan diameter once the spudcan has penetrated about one spudcan diameter into the soil. The latter value is consistent with the diameter of the remoulded zone assumed for the starboard crater model described later.

The predicted spudcan resistance is plotted as a function of depth on Figure 13. From these results it can be observed that a punch-through is initiated at around 7 m, under a preload of about 57 MN. The resistance drops about 10 MN during this punch-through, and does not return to 57 MN until the spudcan has penetrated to around 14 m. A further punch-through is initiated at around 20 m under a preload of about 85 MN, with around a 20 MN maximum drop in leg load; the applied preload is not recovered until the spudcan has penetrated to around 23 m. Thereafter there is only a small additional penetration as the preload is increased to the maximum value actually applied (i.e. 98 MN). The leg load must then be increased to around 120 MN before the next punch-through is initiated in the analysis. For the punch-through commencing at 20 m, a leg run of 3 m is predicted in the LDFE analysis as compared with the observed ‘free fall’, which ranged from about 2.5 m to 5 m at the different legs. During the first punch through, the foundation collects and traps the sand layer at 3 m, which forms a bigger “combined” foundation mobilising a larger volume of soil. This downward movement of the sand layer seems to somewhat delay triggering of the first punch-through event. As the spudcan penetrates deeper, the collected drained sand layer is eroded away by the underlying material and hence at the “trough” of the first punch-through none of this sandy material remains visibly attached to the spudcan.

It can be seen from the operative strength plots that both punch-through events lead to shear band formation. As the spudcan steadily approaches the shear band zone, strain concentrations develop, and hence by the time that the spudcan is in close proximity to these zones the soil strength directly below is extensively degraded. It is this degradation that leads to the relatively low resistances in the punch-through troughs.

Figure 13 also presents the measured spudcan penetration resistance profiles as extracted directly from Ensco records for each leg, and the inferred “average” resistance profile developed by Rupert Hunt. In general, the LDFE predictions agree well with the measurements, bearing in mind that all of the measurements are subject to some uncertainty in interpretation.

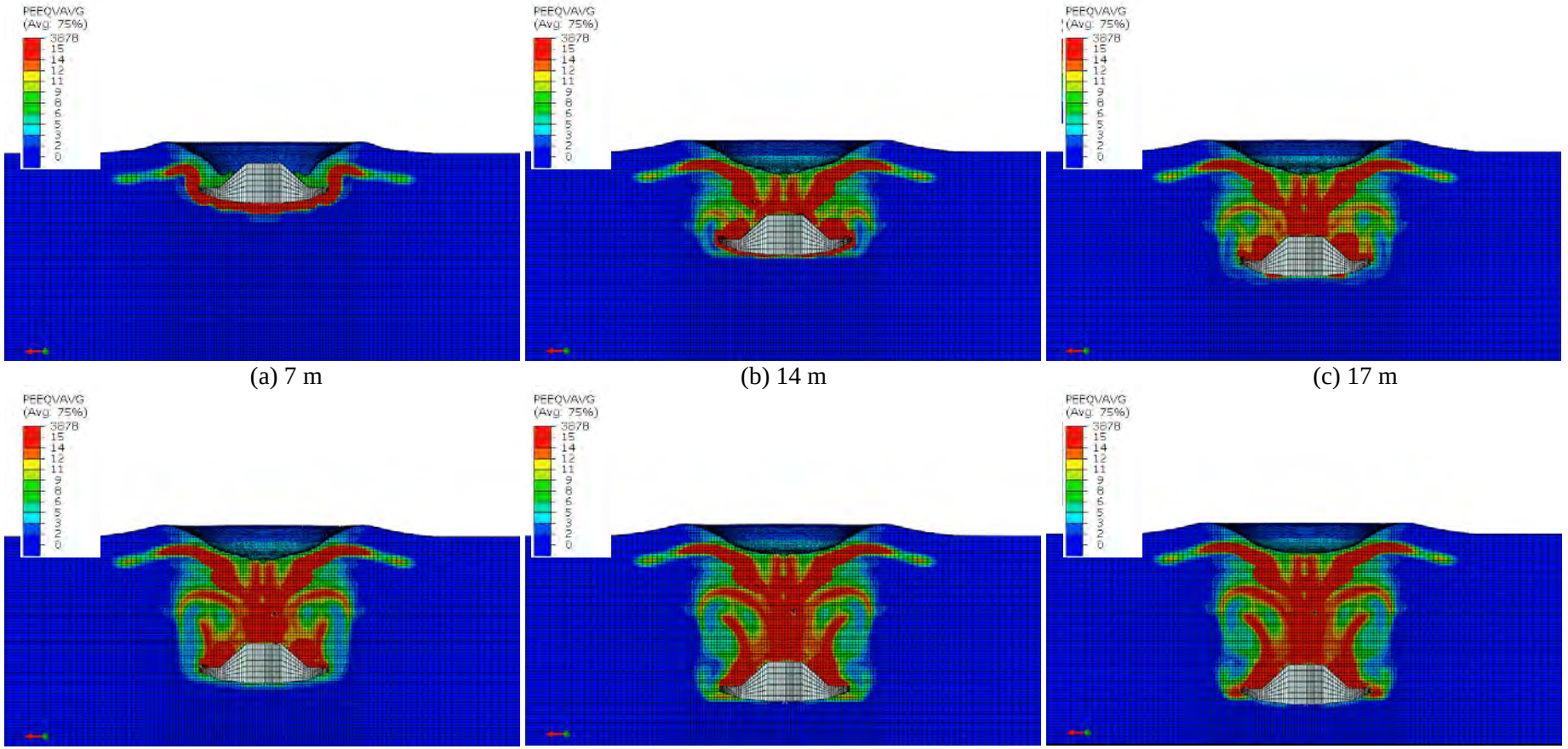

(a) 7 m (b) 14 m (c) 17 m

(d) 20 m (e) 23 m (f) 25 m

Figure 12: Contours of the accumulated plastic strain on central vertical plane for E102 model

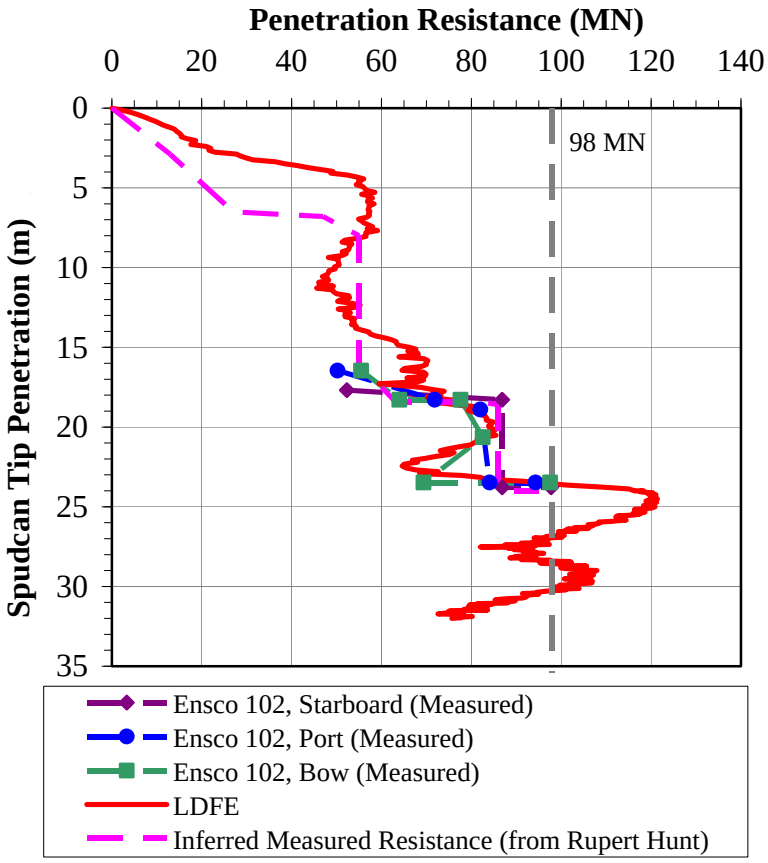

Figure 13: Predicted spudcan penetration resistance for the E102 case

Comparing the LDFE and analytical predictions (see Figure 6) it can be seen that some of the detailed features observed in the LDFE simulation are not well captured using the analytical model. Specifically, the analytical model under-predicts the penetration resistance at shallower depths (i.e. <10 m) due to a combination of less load-spreading and no entrapment/ transporting down of sand below the spudcan. As a result, the analytical model only predicts a small leg run (from about 5 m to 7 m penetration), with a modest gradient of increasing resistance down to around 17 m penetration. The analytical model also predicts a more modest punch-through between 21.5 m and 23 m as compared to the LDFE prediction. This is attributed to the fact that while the effect of remoulding is included in our analytical solution in an average sense (i.e. we scale down the applicable bearing capacity factor to allow for the progressive degradation that develops as soil flows around the spudcan), it cannot capture the observed "action-at-a-distance" effect, where significant strain softening is initiated well ahead of the spudcan during a punch-through event, leading to significant strength reduction by the time that the spudcan has moved down to that depth (as can be noted from Figure 11). The larger reductions in leg load during punch-through that occur in the LDFE compared to the analytical solution are also due to the "action-at-a-distance" effect. Finally we note that as a result of the lower degree of load spreading in the analytical model compared to the LDFE, the predicted penetration resistance at 25 m is only around 105 MN in the former as compared to about 120 MN in the latter. This extra resistance from the LDFE analysis provides useful reassurance that the E102 was probably less marginally balanced under the maximum static preload than the analytical model suggests.

13 LDFE MODEL – DESCRIPTION & RESULTS; STARBOARD CRATER

In order to keep run times to a manageable level, the soil domain for the starboard crater LDFE analyses was divided into two halves, termed “northern half” and “southern half” respectively. The vertical axis dividing these halves was selected after inspection of the CPT resistance profiles comprising each half, such that there was an approximate “balance” between the average strength of the two halves; the selected split is shown on Figure 14. Separate analyses were then conducted for the two halves.

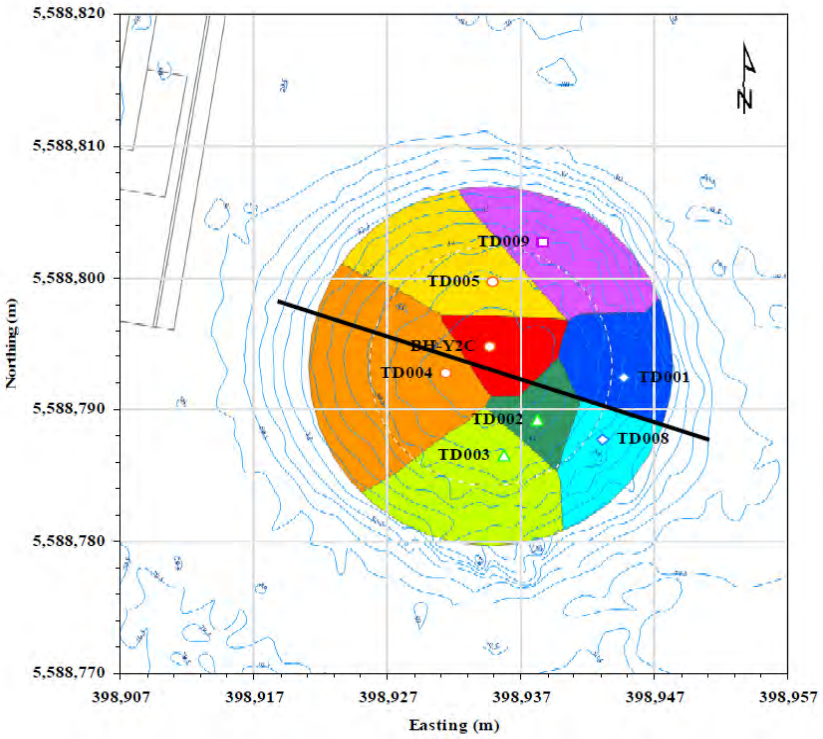

Figure 14: Investigated PCPT Locations and Material Zoning- Starboard Crater

The mesh used for the starboard crater analyses is presented on Figure 15. Compared to the in situ E102 case there are some notable differences:

- The top 1.6 m of material, which only exists at and beyond the outer extremities of the crater, was not modelled explicitly since it has negligible influence on the final results. Instead we imposed a surcharge of 11.2 kPa on the top soil surface to represent the weight of the missing soil.
- The southern half crater runs were conducted first, with the mesh base assigned at 29 m below the original mudline. *A-priori*, this was thought to be sufficiently deep, but after reviewing the first set of results it was apparent that a deeper mesh was required to properly model the response for spudcan penetration deeper than 24 m. The northern half crater analyses were therefore conducted with the mesh base defined at 33.6 m below mudline (i.e. same as used for the E102 in situ case).
- The soil material was incorporated into the Eularian mesh accounting for the existing hemispherical crater surface topography.
- The West Telesto spudcan geometry was adopted instead of the E102.

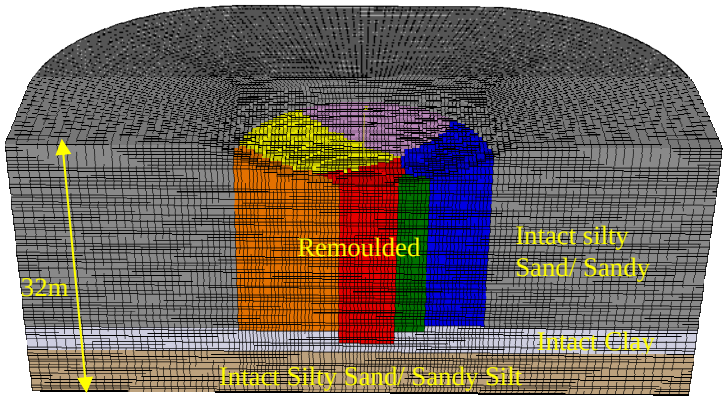

Figure 15: Mesh Adopted for Re-penetration LDFE Analyses

In order to provide a representative range for the potential spudcan penetration within the starboard crater, analyses were conducted for three scenarios:

- 'Scenario 1': All the soil units were treated as undrained/ partially drained ('cohesive' material model);
- 'Scenario 2': The sandy units were modelled as a frictional material (ϕ'= friction angle, ψ'=dilation angle); the rest of the soil was modelled undrained/ partially drained ('cohesive' material model);
- 'Scenario 3': Same as 'Scenario 1' but with a reduced rate of remoulding for the undrained soil.

The key material properties used for each scenario are summarised in the table below.

Scenario	**Remoulded Zone: Tresca**		**Sand: Mohr Coulomb**		**Intact Clay: Tresca**		**Intact Sandy Silt/ Silty Sand: Tresca**	
	ζ_{95}	S_t	ϕ'	ψ	ζ_{95}	S_t	ζ_{95}	S_t
1	3	4	n/a	n/a	15	4	8	15
2	3	4	35	5	15	4	8	15
3	15	4	n/a	n/a	15	4	8	15

The range of ξ_{95} values adopted for the remoulded crater material were intended to account for differing assumptions as to the relative importance of diffuse shearing; the larger value is essentially half the best estimate measured value (i.e. 30), which is consistent with the assumption adopted for the E102 analyses. The factor of 10 is considered more realistic where shear bands dominate during punch-through but will overestimate the rate of strain softening in all soil zones subject to diffuse shear. Some additional sensitivity analyses were also conducted varying various parameters, but these are not discussed in this paper.

Representing a typical example, Figures 16 and 17 show static images presenting contours of the operative undrained strength on the central vertical plane of the model and on a 90-degree quadrant, respectively, at various stages during the penetration process for the northern half analysis (Scenario 1). Figure 18 presents the accumulated plastic strain contours at the same depths.

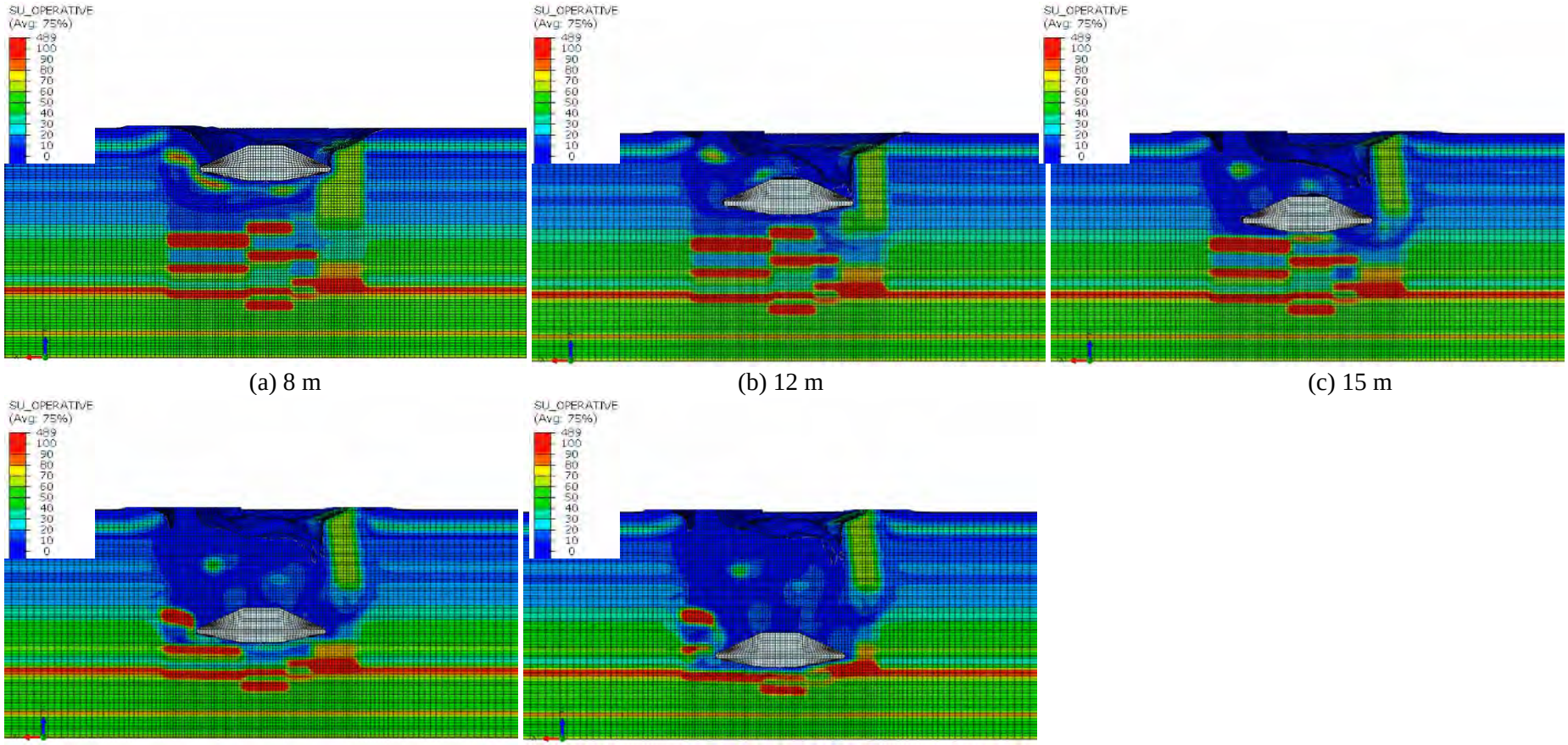

(a) 8 m (b) 12 m (c) 15 m

(d) 20 m (e) 23.3 m

Figure 16: Contours of the operative undrained strength on central vertical plane for Northern Half Crater Model (Scenario 1)

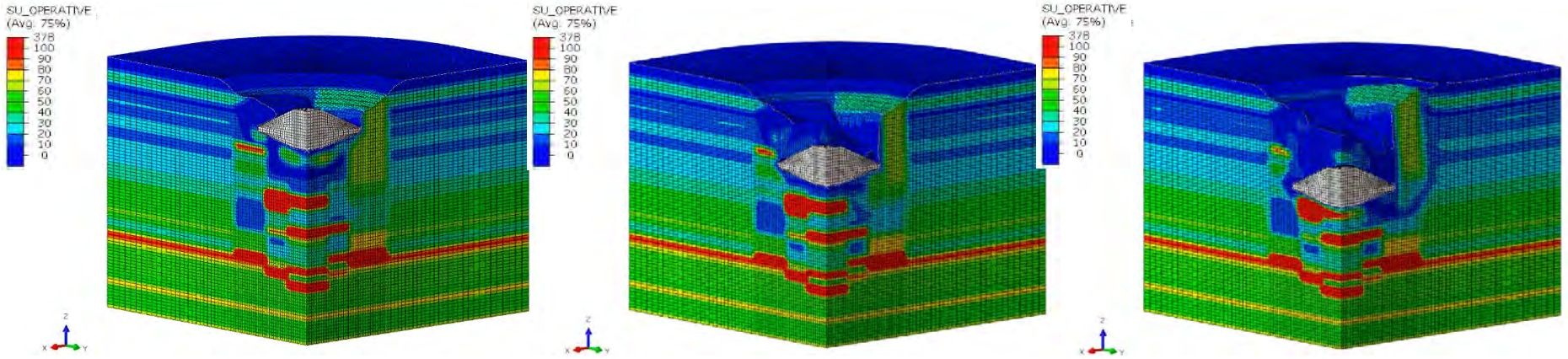

(a) 8 m (b) 12 m (c) 15 m

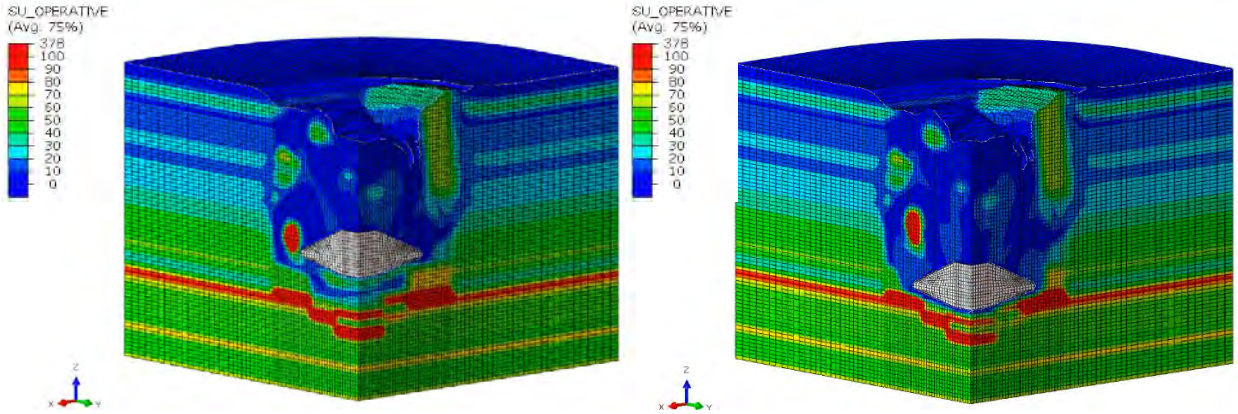

(d) 20 m (e) 23.3 m

Figure 17: Contours of the operative undrained strength on a 90-degree quadrant for Northern Half Crater Model (Scenario 1)

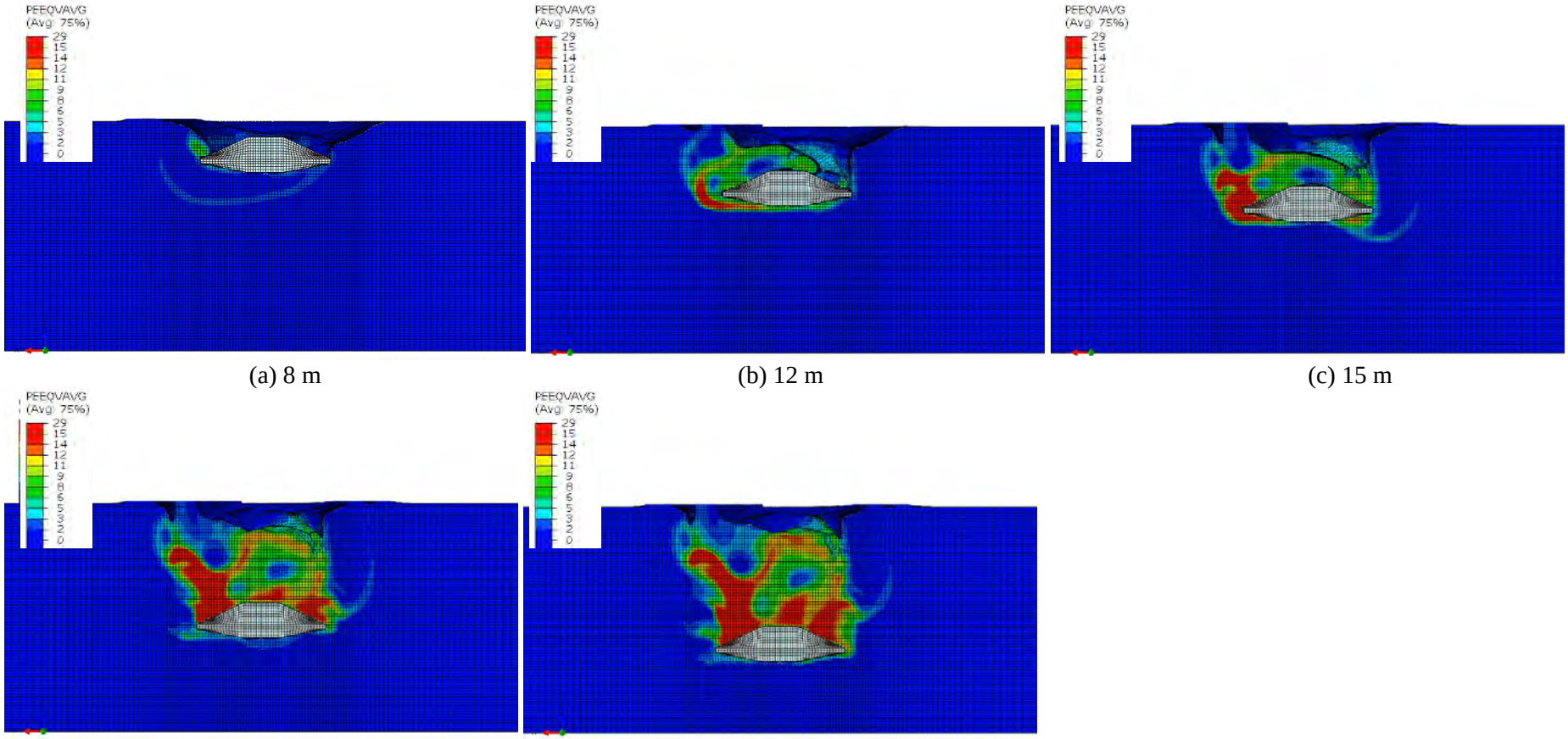

(a) 8 m (b) 12 m (c) 15 m

(d) 20 m (e) 23.3 m

Figure 18: Contours of accumulated plastic strain on the central vertical plane for Northern Half Crater Model (Scenario 1)

It can be seen from the plots of operative strength that the stronger material within each zone initially appears to spread load thereby enhancing the penetration resistance. However, in all cases as the spudcan penetration proceeds these reinforcing layers are gradually displaced radially outwards and degraded to a lower strength, which eventually eliminates any reinforcing effect.

The penetration resistance is plotted versus depth on Figure 19 for this case. For ease of presentation and comparison purposes, it should be noted that the presented resistance has been doubled from the value calculated for the actual half crater model; this inherently implies that the northern half crater soil is mirrored in the southern half.

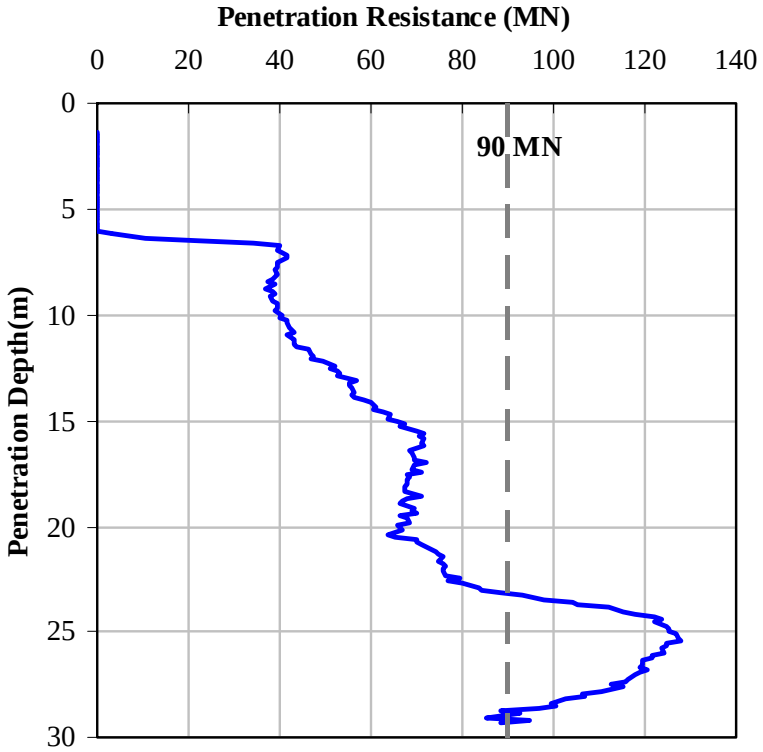

Figure 19: Penetration Resistance for Northern Half Crater Model (Scenario 1)

It can be observed that an initial punch-through is initiated at around 7 m penetration under a preload of about 40 MN, while a more significant punch-through is initiated at ~15 m when the spudcan encounters a number of sand lenses sandwiching softer materials. The increase in spudcan penetration resistance from 8 m to 12 m is due to the influence of a higher strength zone (e.g. see TD001) and some inter-bedded sand pockets. The edge of the spudcan cuts through this stronger zone resulting initially in a one-sided failure mechanism towards the weaker side. When the spudcan reaches about 12 m, a deep-seated shear band forms below the strongest zone within the TD001 profile and triggers a global 2-sided failure mechanism mobilising a greater volume of soil around the spudcan. A significant increase in penetration resistance is observed as the spudcan moves from 12 m to 15 m as the main grouping of sand lenses/ pockets is approached. At a penetration depth of 15 m, intense shearing of weak zones between the various sand lenses/ pockets leads to substantial remoulding of these weak materials, leading to a drop in resistance with increasing penetration. The resistance picks up again once the spudcan has penetrated deeper than around 20 m. The final penetration depth achieved under 90 MN preload is 23.3 m. At even greater depths there is a pronounced increase in resistance, which is very similar to that achieved in the E102 back-analysis. It should be noted that a similar increase did not occur in the equivalent southern half crater analysis due to the insufficient base depth adopted in that case.

As already noted, the total penetration resistance presented above was computed by doubling the half model penetration resistance. However, in practice the spudcan will simultaneously see a northern and southern half crater and hence the overall load-penetration response should be obtained by summing the resistance from the two halves of equivalent scenarios. Figure 20 presents the individual southern and northern half crater results for each of the three basic scenarios outlined earlier and the combined spudcan penetration results obtained by summing the two halves. Potential leg runs are identified on the plots in each case as well as the predicted final penetration under the maximum design preload of 90 MN. Finally we have also included the analytical model predictions made using Method 1.

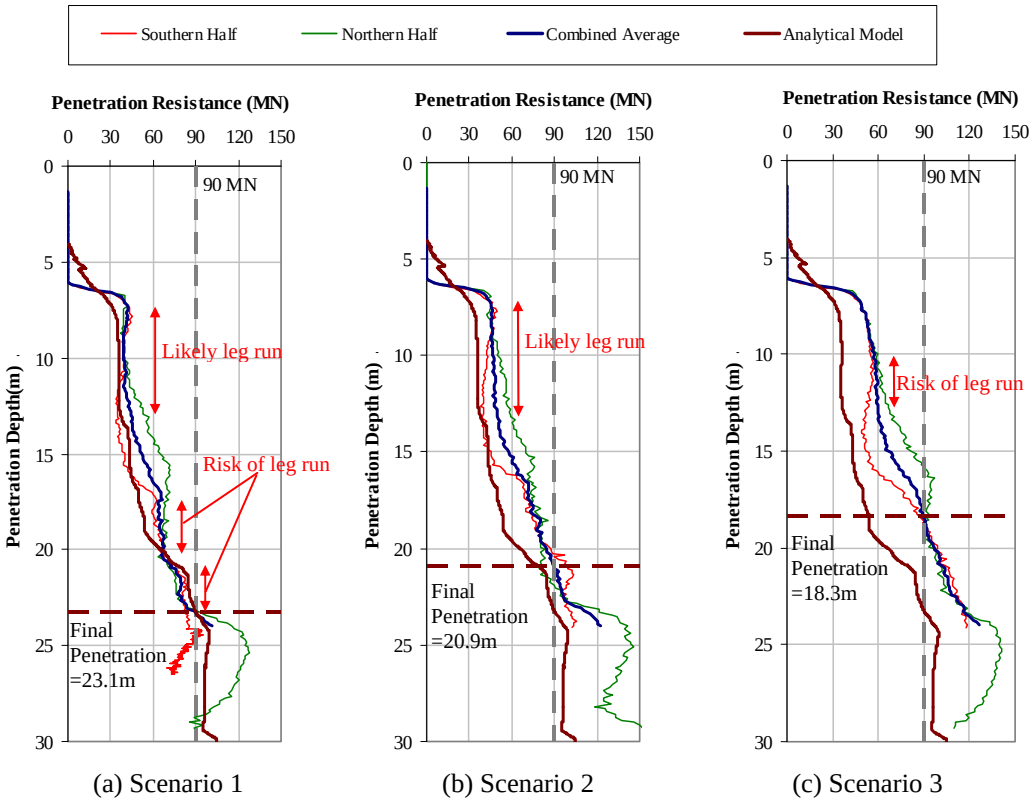

(a) Scenario 1 (b) Scenario 2 (c) Scenario 3

Figure 20: Combined Spudcan Penetration Results

The following conclusions can be drawn from these results:

- While a number of potential leg runs are identified, all but one occur at preloads less than the 70 MN hull-in-water simultaneous leg jacking limit. Under these conditions the leg will simply continue to be jacked down but with a minor loss of draft as the trough of the resistance is reached.
- The one exception is for Scenario 1 at 80 MN between 21 m and 22 m. However, this does not involve any significant reduction in leg load so should be readily arrested provided the hull remains in the water during preloading.
- A range of final leg penetrations are identified; varying from 23.1 m for Scenario 1, to 18.3 m for Scenario 3. The former is very similar to the penetration achieved previously with the Ensco 102 in virgin soil, but the latter is much less. The enhancement of resistance for Scenario 2 compared to Scenario 1 is due to the greater robustness of the sand pockets when modelled with frictional properties – their strength is not degraded as they are strained, so they must be transported down and/ or pushed out of the way. The enhancement for Scenario 3 is due to the reduced rate of strain softening that is imposed in that case.

- The overall response and the final penetration depths under a 90 MN preload (~23.2 m) obtained from the analytical model (Figure 8) are very similar to LDFE Scenario 1.

14 COMPARISON WITH FIELD OBSERVATIONS

The rig move to Yolla occurred at the end of February 2015 and proved to be a text book operation. The spudcan reaction and penetration depths measured are presented on Figures 21, 22 and 23 for the bow, port and starboard legs, respectively. Also shown on these figures are the analytical model predictions and, for the starboard leg, the LDFE predictions. Note that for the port leg, two analytical predictions are presented since two CPT's were conducted in this crater. It can be seen that the measured data generally agrees well with the analytical model predictions, particularly at the bow and port legs. At the starboard leg, the measured spudcan penetrations under a preload of 40 MN to 50 MN is notably deeper than the analytical model prediction. Nonetheless, the general trend of the penetration depth – reaction curve was captured by the analytical model. For the starboard leg the resistance determined from the various LDFE analyses are generally significantly higher than the measured data. In the 3D LDFE model (and the analytical model) a significant number of sand lenses (as measured by the various CPTs) were conservatively modelled as extending beyond the spudcan footprint. However, the measured data appears to demonstrate that the sand lenses were actually confined to the region directly under the Ensco 102 spudcan footprint, since the lower observed resistance does not support the load spreading effects that resulted from modelling extended sand lenses. Support for this conclusion was also found by comparing the measured data at the starboard crater with the individual spudcan penetration curves calculated for each PCPT probe at the starboard leg (Figure 8). It was found that the measured data agrees well with the lower bound of all the calculated curves, which implies that the failure mechanism at each depth was controlled by the weak matrix material with minimal influence from the interleaved sand lenses.

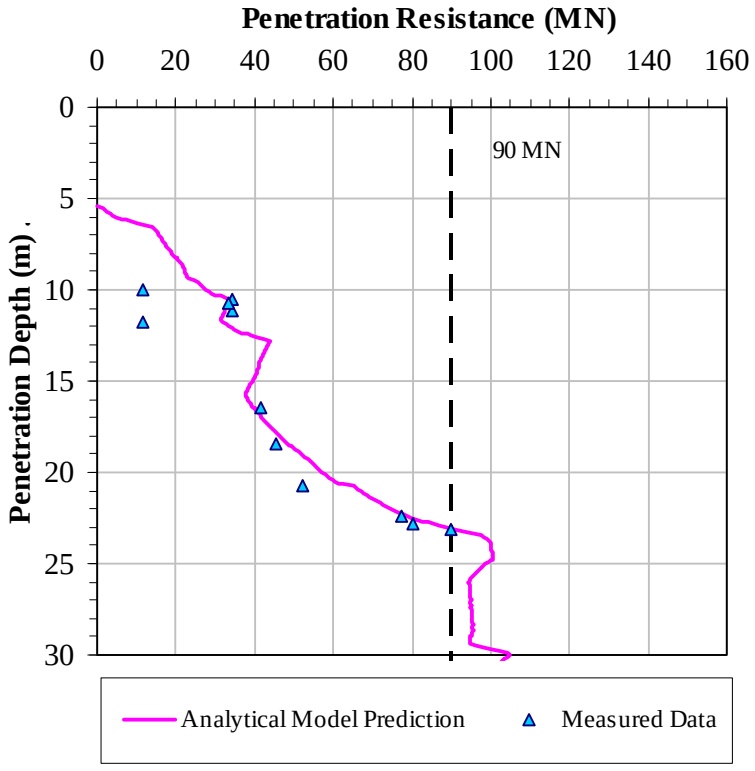

Figure 21: Measured Data and Prediction of Spudcan Penetration (Bow Leg)

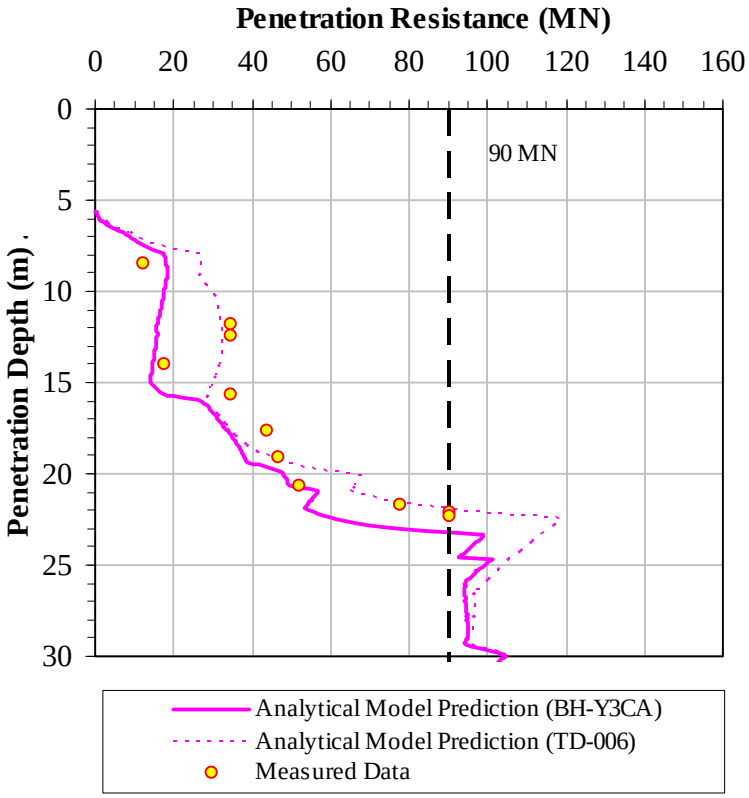

Figure 22: Measured Data and Prediction of Spudcan Penetration (Port Leg)

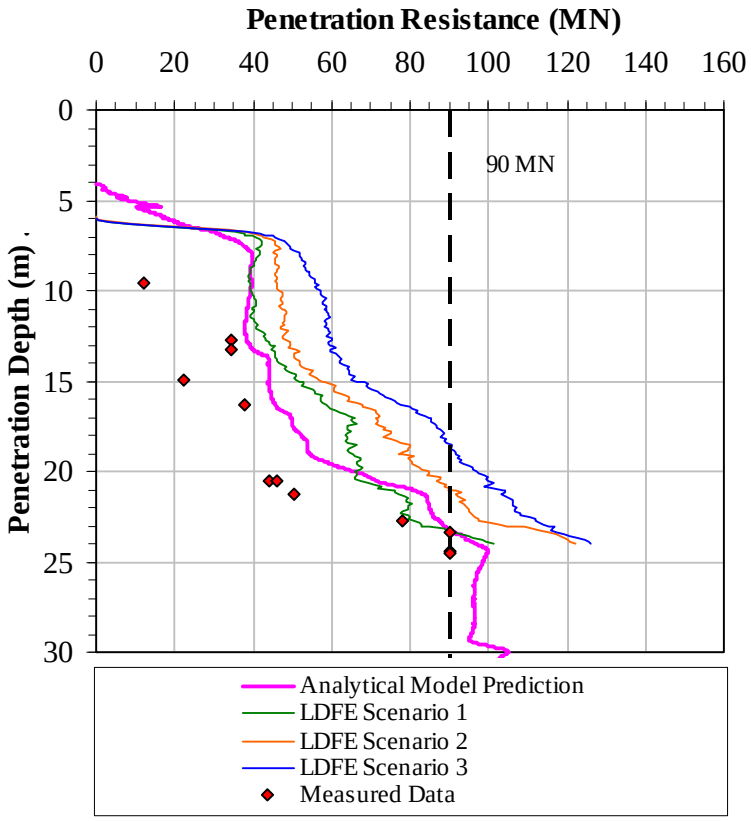

Figure 23: Measured Data and Prediction of Spudcan Penetration (Starboard Leg)

15 CONCLUSIONS

The work presented in this paper was conducted as part of a comprehensive engineering evaluation that may be unprecedented in the history of global jack-up installations. The lessons learnt from the surprises and near-miss that occurred with the E102 in 2004 were well learnt and no stone was left unturned to minimise the risk of undesirable outcomes this time. The success of the field installation operations confirm that all the key risks were identified and appropriately mitigated. Nevertheless, despite the comprehensive site investigation data collected and analysis performed, the details of the actual West Telesto penetration response at the starboard crater still provided some modest surprises; most notably in that this spudcan penetrated deeper than all the others. An explanation has been provided for the observed behaviour, but this once again confirms there is no room for complacency whenever one encounters highly sensitive carbonate silty soils with transitional drainage conditions.

16 ACKNOWLEDGEMENTS

The authors would like to thank the BassGas Joint Venture partners for permission to publish this paper. Origin Energy is the Operator of the BassGas Joint Venture in permit T/L1.

The BassGas Joint Venture partners in T/L1 are:

Origin Energy Resources Limited (Operator)	42.50%
AWE Limited (via subsidiaries)	35.00%
Toyota Tsusho Gas E&P Trefoil Limited	11.25%
Prize Petroleum International Pte. Ltd	11.25%

The success of the West Telesto operations at Yolla can be attributed to the team Origin put together for this exercise, and the contributions made by DNV-GL, Halliard Consulting, Seadrill and the various technical experts from the Yolla partners are acknowledged.

17 REFERENCES

[1] Erbrich CT., Australian Frontiers – Spudcans on the Edge. in: Proceedings, The International Symposium on Frontiers in Offshore Geotechnics (ISFOG)., Australia 2005., p.49-75.

[2] SNAME., Guidelines for Site Specific Assessments of Mobile Jack-up Units., The Society of Naval Architects and Marine Engineers., New Jersey 2008.

[3] Salençon J. and Matar., Capacité Portant des Fondations Superficielles Circualires. Journal de Méchanique Theorique et Appliqué, 1982, Vol. 1, No. 2, p 237-267.

[4] Amodio A., Erbrich CT., Murugavel V. and Moyle I., Re-visiting Yolla – Managing Storm Stability; Geotechnical Assessment. in: Proceedings, International Conference: The Jack-up Platform., London, UK, 2015.

[5] DSIMULIA. ABAQUS Version 6.13, User Manual. 2013.

[6] Tho KK., Leung CF., Chow YK. and Swaddiwudhipong S., Eularian Finite-Element Technique for Analysis of Jack-up Spudcan Penetration. International Journal of Geomechanics, ASCE, 2012, Vol. 12, No. 1.

[7] Einav I. and Randolph MF., Combining Upper Bound and Strain Path Methods for Evaluating Penetration Resistance., International Journal for Numerical Methods in Engineering, 2005, Vol. 63, Issue 14.